Supporting Information

Ag/Pd bimetallic nanoparticles loaded Zr-MOF: An efficacious visible light responsive photocatalyst towards H_2O_2 and H_2 production

Srabani Dash[a], Suraj Prakash Tripathy[a], Satyabrata Subudhi[a], Lopamudra Acharya[a], Asheli Ray[a], Pragyandeepti Behera[a], Kulamani Parida[a]*

[a] Centre for Nano Science and Nanotechnology, Siksha 'O' Anusnadhan (Deemed to be University), Bhubaneswar, Odisha, 751030, India

(*Corresponding Author)

(*The following electronic supporting information contains 8 pages, 04 tables, and 5 figures*.)

---

* Corresponding author E-mail: paridakulamani@yahoo.com, kulamaniparida@soa.ac.in,
Tel. No. +91-674-2351777, Fax. +91-674-2350642

1. Experimental Techniques:

1.1. Characterization Techniques:

The powder X-ray diffraction (PXRD) analysis was carried out by using Rigaku Ultima-IV (40 kV-40 mA) which is connected with Cu Kα source having radiation (λ = 0.154 nm) at 2θ range (5°-80°) to detect the crystallinity and phase purity properties of the material. Fourier transform infrared (FTIR) spectrometer analysis was carried out with JASCO FTIR-4600-LE taking KBr (potassium bromide) as reference for interpretation of the functional groups of synthesized materials between the range of 4000-400 cm^{-1}. To determine the oxidation states and chemical composition of the materials X-ray photoelectron spectroscopy (XPS) analysis was performed by VG-microtech-multilab-ESCA-3000 spectrometer (Mg-K-X-ray non-monochromatized source). By the Brunaure–Emmett–Teller (BET) surface area analysis and the N_2 adsorption-desorption evaluation materials textural properties were measured using NOVA-2200e Quantachrome analyser. The surface morphology was analyzed by scanning electron microscopy (SEM) with 200 kV JEOL-JEM-2100 that was coupled with energy-dispersive X-ray (EDS) and elemental mapping analysis apparatus respectively and the internal topology of the produced photocatalysts, were analyzed through transmission electron microscopy (TEM) by ZEISS SUPRA-55. The optical characteristics of the synthesized samples were measured using a JASCO-V-750 UV-Visible spectrophotometer with $BaSO_4$ reference in the wavelength range (200-800 nm). The excitation and emission spectra of photoluminescence (PL) were measured using a JASCO FP-8300 fluorescence spectrometer using Xenon lamp as the light source with an excitation wavelength of 325 nm. The TRPL analysis was carried out by Edinburgh-FLS920 Fluorescence spectrometer which is coupled with a multi-channel scaling (MCS) module fitted to the F290H pulsed Xe microsecond flash lamp source. Electrochemical properties of the prepared materials were characterized by using IVIUMnSTAT multi-channel analyzer. Furthermore, Agilent Technology gas-chromatography was used to analyze the evolution of H_2 (GC-7890B). An ICP-OES elemental analyzer (Elementar Vario EL III Carlo Erba 1108) was used to determine the loading percentage of the elements present.

1.2. FTO Preparation: Additionally, the prepared materials were dropcastingly deposited on the fluorine-dopped tin oxide (FTO) glass. Firstly, the FTO glasses were ultrasonically washed with DI and ethanol for 20 min each and then dried at 75 ^{o}C. The suspension which comprised of distilled water (1.6 mL), ethanol (1.4 mL) and Nafion (40 μL) was uniformly coated on the conducting surface of FTO. The Ag/AgCl taken as reference electrode, Pt electrode used as

counter electrode, and the sample coated FTO as working electrode were installed three electrode based electrochemical cell and by taking Na_2SO_4 (0.2 M) as electrolyte.

1.3. Scavenger Test Procedure: Radical scavenger tests were carried out to clarify the reactive species in charge of the production of H_2O_2 by (1:2) Ag/Pd@UiO-66-NH_2 under light illumination. These experiments are depicted in (Fig. S4) The influence of $^{\bullet}O_2^-$, $OH^{\bullet}$, h^+, and e^- species on photocatalytic H_2O_2 formation was investigated using 1,4-benzoquinone (PBQ), isopropanol (IPA), citric acid (CA), and dimethyl sulfoxide (DMSO), in that order. When PBQ and DMSO were introduced to the photocatalytic system, the yield of H_2O_2 was dramatically reduced, confirming the considerable contribution of both $^{\bullet}O_2^-$ and e^- via indirect and direct O_2 reduction routes. Also, the addition of IPA showed a significant impact on H_2O_2 production which exhibit the remarkable role of $OH^{\bullet}$ radicals. Moreover, the significant H_2O_2 yield delay caused by the addition of CA showed a minor involvement of h^+ radicals as reactive intermediate species during the photocatalytic H_2O_2 production process.

Fig S1: BET surface area (Inset: BJH pore size distribution) of (1:2) Ag/Pd@UiO-66-NH_2

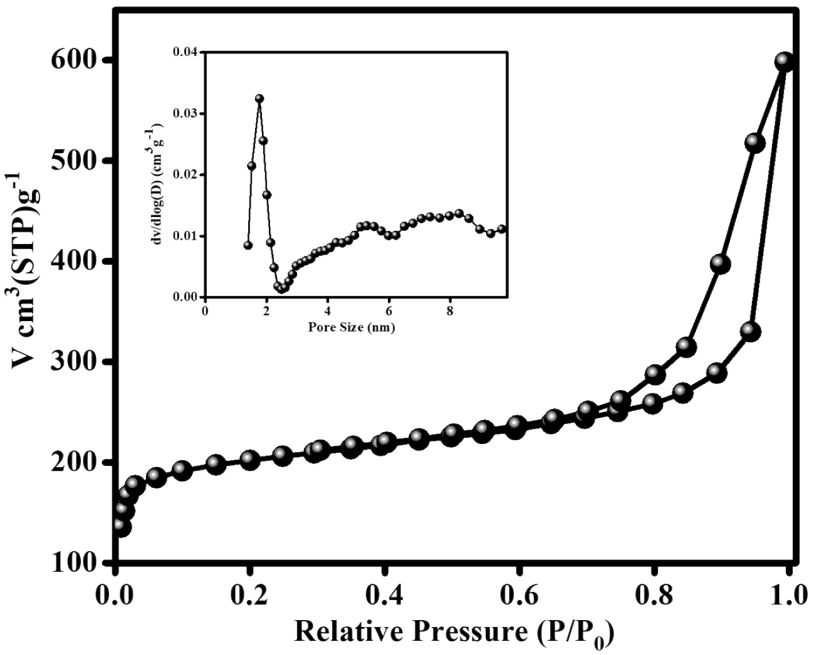

Fig. S2: Survey XPS spectrum of pristine UiO-66-NH_2 and composite (1:2) Ag/Pd@UiO-66-NH_2

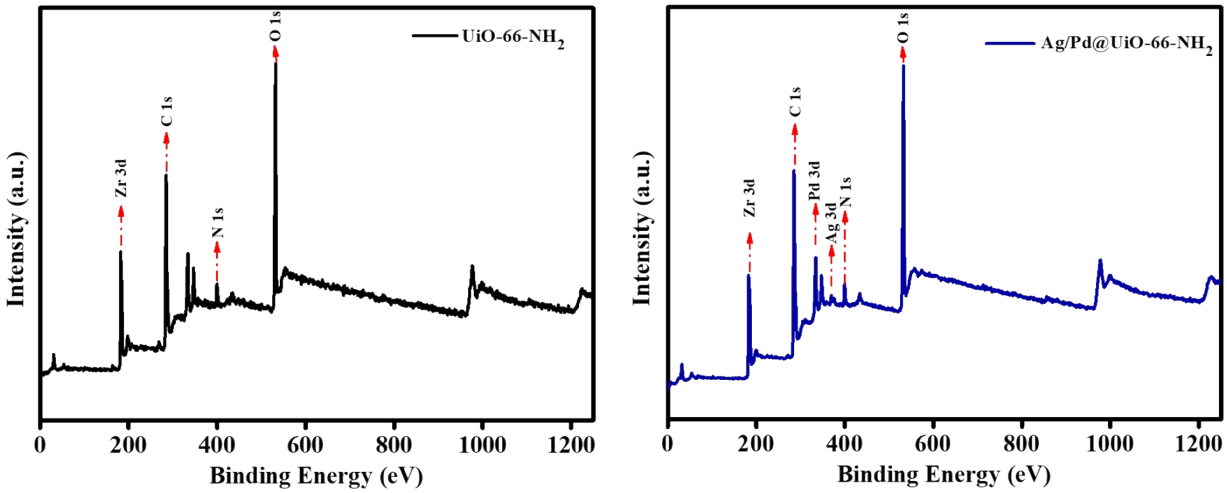

Fig. S3: PL plot for pristine UiO-66-NH_2 and (1:1, 1:2, 2:1) Ag/Pd@UiO-66-NH_2

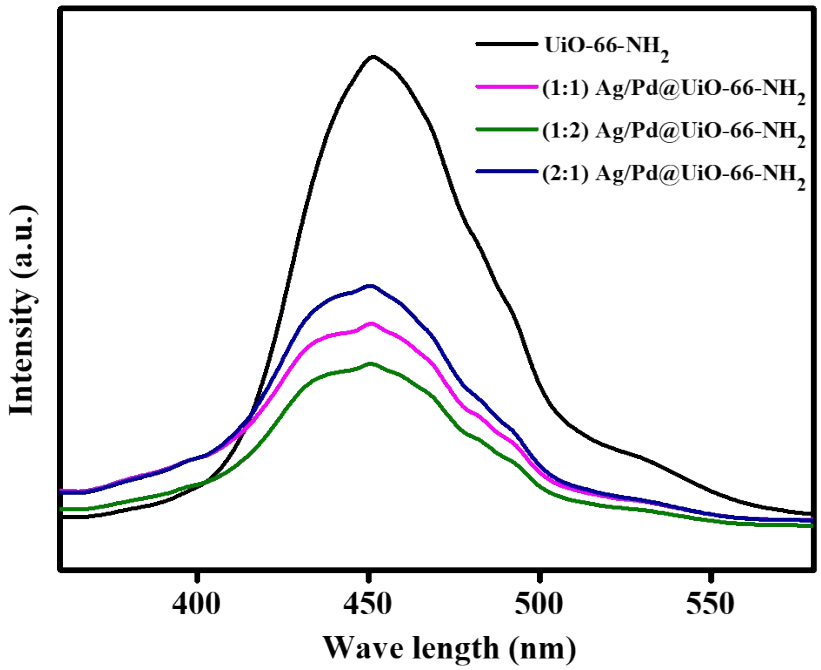

Fig. S4: TRPL plot of (1:2) Ag/Pd@UiO-66-NH_2

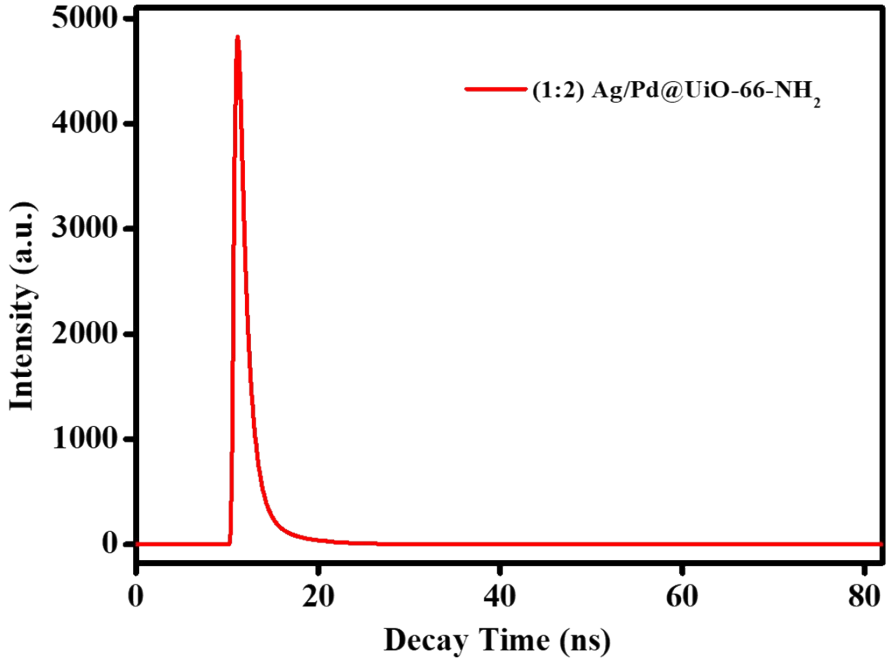

Fig. S5: LSV plot of the prepared photocatalysts

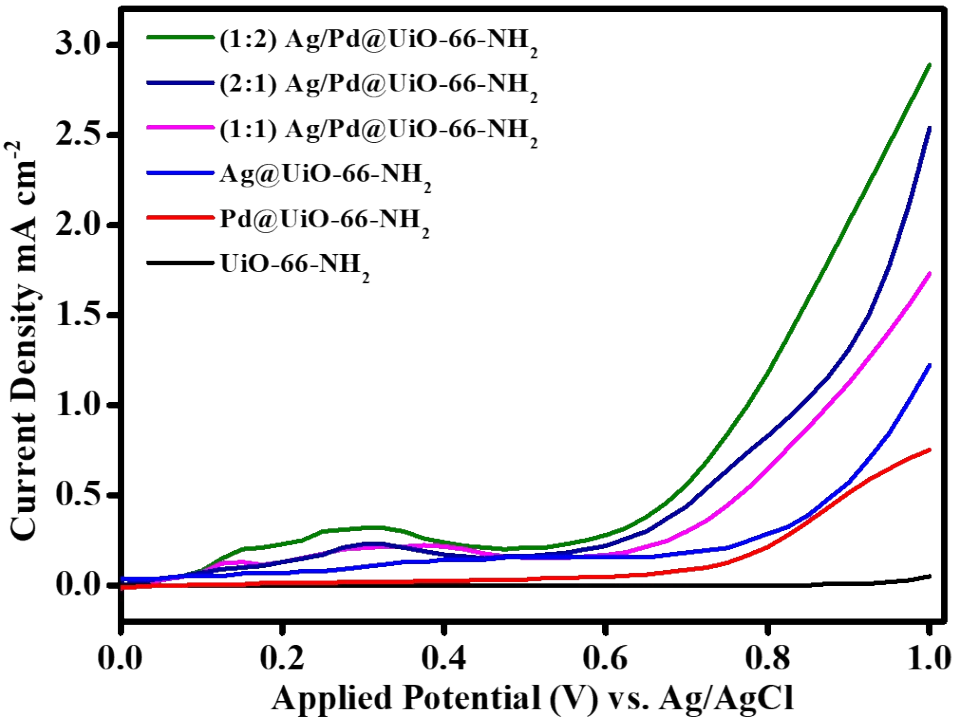

Fig. S6: Post photo-catalytic PXRD analysis

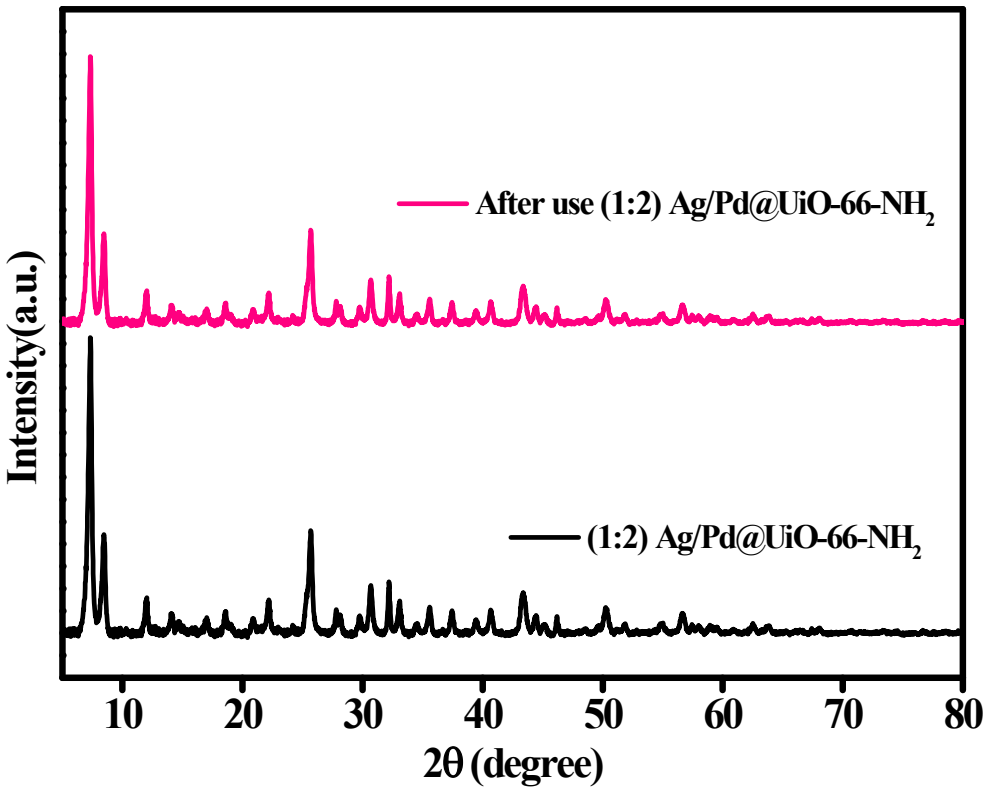

Table S1: TRPL fitting data and average life times of the prepared MOFs

Sample Name	τ_1	τ_2	**A1**	**A2**	τ_{avg}	**Ref.**
UiO-66-NH_2	0.36	4.81	6600.48	16.40	0.504	[1]
(1:2) Ag/Pd@UiO-66-NH_2	0.81	6.82	63.6	21.76	0.537	***This study***

Table S2: Apparent Conversion Efficiency (ACE) Expression and Calculation for photocatalytic hydrogen evolution by the prepared photocatalysts

ACE Expression	**ACE Value**
ACE (H_2) = $\frac{stored\ chemical\ energy\ (SCE)}{incident\ light\ intensity\ (ILI)}$ ACE (H_2) = $\frac{moles\ of\ H\ produced\ (in\ \mu mol/s)\ \times\ \Delta H}{150 mW\ cm^{-2} \times (area\ of\ the\ spherical\ surface\ on\ wh}$ [ΔH_c = Heat of Combustion (kJ mol^{-1}) for $H_2 = 2H^+ + ½ O_2$; ΔH_c = 285.8 kJ mol^{-1}, r = Circle radius = 1.5 cm.]	$ACE_{(UNH)}$: 0.88 % $ACE_{(1:2)Ag/Pd@UiO-66-NH2}$: 3.30 %

Table S3: Comparative table for photocatalytic H_2O_2 production by various photocatalysts

Sl. No.	Material Name	Light Source	H_2O_2 Production	Ref.
1.	Hexagonal rosettes g-C_3N_4	Visible light (λ > 420 nm)	150 μmol h^{-1} g^{-1}	[2]
2.	CoP/g-C_3N_4	Visible light (λ > 420 nm)	140 μmol in 2 h	[3]
3.	PEI/g-C_3N_4	Visible light (λ > 420 nm)	208.1 μmol h^{-1} g^{-1}	[4]
4.	$Bi_4O_5Br_2$/g-C_3N_4	Visible light (λ > 420 nm)	124 μmol h^{-1}	[5]
5.	CdS/rGO	Sun light	164 μmol h^{-1}	[6]
6.	Ti_3C_2/TiO_2	Visible light (λ > 420 nm)	179.7 μmol L^{-1} h^{-1}	[7]
7.	Ag/$ZnFe_2O_4$-Ag-Ag_3PO_4	Visible light (λ > 420 nm)	206.3 μmol L^{-1}	[8]
8.	O−CNC	Visible light (λ > 420 nm)	2008.4 μmol h^{-1} g^{-1}	[9]
9.	DCN-15A	Visible light (λ > 420 nm)	12.1 μmol h^{-1}	[10]
10.	(1:2) Ag/Pd@UiO-66-NH_2	Visible light (λ > 420 nm)	39.4 μmol h^{-1}	***This study***

Table S4: Comparative table for photocatalytic H_2 evolution by various photocatalysts

Sl. No.	Material Name	Light Source	H_2 Production	Ref.
1.	NU66/ZIS	300 W Xe lamp (λ ≥ 420 nm)	2199 μmol h^{-1} g^{-1}	[11]
2.	Pt@UiO-66-NH_2@$ZnIn_2S_4$	300 W Xe lamp (λ ≥ 420 nm)	850 μmol h^{-1} g^{-1}	[12]
3.	Au_4@UiOS@ZIS	300 W Xe lamp (λ ≥ 420 nm)	391 μmol h^{-1}	[13]
4.	PtNi/g-C_3N_4	300 W Xe lamp (λ ≥ 420 nm)	104.7 μmol h^{-1}	[14]
5.	Ag-Pd/ZIS	300 W Xe lamp (λ ≥420 nm)	125.4 μmol h^{-1}	[15]

6.	Cu-Pt/SrTiO3	Visible Light ($\lambda \geq 420$ nm)	369.4 μmol h^{-1}	[16]
7.	AuPd/g-C_3N_4	Visible light ($\lambda \geq 420$ nm)	2145 mmol h^{-1} g^{-1}	[17]
8.	Au/g-C_3N_4	Visible light ($\lambda \geq 420$ nm)	423.1 μmol h^{-1}	[18]
9.	CdS/PdAg/g-C_3N_4	300 W Xe lamp ($\lambda \geq 420$ nm)	3098.3 μmol h^{-1} g^{-1}	[19]
10.	(1:2) Ag/Pd@UiO-66-NH_2	300 W Xe lamp/Visible Light	448.2 μmol h^{-1}	***This study***

References:

1 S. P. Tripathy, S. Subudhi, A. Ray, P. Behera, J. Panda, S. Dash and K. Parida, *J Colloid Interface Sci*, 2023, **629**, 705–718.

2 T. Mahvelati-Shamsabadi, H. Fattahimoghaddam, B. K. Lee, S. Bae and J. Ryu, *J Colloid Interface Sci*, 2021, **597**, 345–360.

3 Y. Peng, L. Wang, Y. Liu, H. Chen, J. Lei and J. Zhang, *Eur J Inorg Chem*, 2017, **2017**, 4797–4802.

4 X. Zeng, Y. Liu, Y. Kang, Q. Li, Y. Xia, Y. Zhu, H. Hou, H. Uddin, T. R. Gengenbach, D. Xia, C. Sun, D. T. Mccarthy, A. Deletic, J. Yu and X. Zhang, *ACS Catal.* 2020, **6**, 3697–3706.

5 X. Zhao, Y. You, S. Huang, Y. Wu, Y. Ma, G. Zhang and Z. Zhang, *Appl Catal B*, 2020, **278**, 119251.

6 X. Li, D. Chen, N. Li, Q. Xu, H. Li and J. Lu, *J Colloid Interface Sci*, 2023, **648**, 664–673.

7 Y. Chen, W. Gu, L. Tan, Z. Ao, T. An and S. Wang, *Appl Catal A Gen*, 2021, **618**, 118127.

8 X. Ma and H. Cheng, *Chemical Engineering Journal*, 2022, **429**, 132373.

9 H. Xie, Y. Zheng, X. Guo, Y. Liu, Z. Zhang, J. Zhao, W. Zhang, Y. Wang and Y. Huang, *ACS Sustain Chem Eng*, 2021, **9**, 6788–6798.

10 L. Shi, L. Yang, W. Zhou, Y. Liu, L. Yin, X. Hai, H. Song and J. Ye, *Small*, 2018, **9**, 1703142.

11 C. Zhao, Y. Zhang, H. Jiang, J. Chen, Y. Liu, Q. Liang, M. Zhou, Z. Li and Y. Zhou, *Journal of Physical Chemistry C*, 2019, **123**, 18037–18049.

12 L. Wang, Y. Zhao, B. Zhang, G. Wu, J. Wu and H. Hou, *Catal Sci Technol*, 2023, **13**, 2517–2528.

13 S. Mao, J. W. Shi, G. Sun, D. Ma, C. He, Z. Pu, K. Song and Y. Cheng, *Appl Catal B*, 2021, **282**, 119550.

14 W. Peng, S. S. Zhang, Y. B. Shao and J. H. Huang, *Int J Hydrogen Energy*, 2018, **43**, 22215–22225.

15 C. Liu, Y. Zhang, J. Wu, H. Dai, C. Ma, Q. Zhang and Z. Zou, *J Mater Sci Technol*, 2022, **114**, 81–89.

16 L. Qin, G. Si, X. Li and S. Z. Kang, *RSC Adv*, 2015, **5**, 102593–102598.

17 C. Han, Y. Gao, S. Liu, L. Ge, N. Xiao, D. Dai, B. Xu and C. Chen, *Int J Hydrogen Energy*, 2017, **42**, 22765–22775.

18 X. B. Qian, W. Peng and J. H. Huang, *Mater Res Bull*, 2018, **102**, 362–368.

19 J. Gao, F. Zhang, H. Xue, L. Zhang, Y. Peng, X. L. Li, Y. Gao, N. Li and G. Lei, *Appl Catal B*, 2021, **281**, 119509.